Continuous Phase Modulation—Part II: Partial Response Signaling

TOR AULIN, MEMBER, IEEE, NILS RYDBECK, AND CARL-ERIK W. SUNDBERG, MEMBER, IEEE

Abstract—**An analysis of constant envelope digital partial response continuous phase modulation (CPM) systems is reported. Coherent detection is assumed and the channel is Gaussian. The receiver observes the received signal over more than one symbol interval to make use of the correlative properties of the transmitted signal. The systems are M-ary, and baseband pulse shaping over several symbol intervals is considered. An optimum receiver based on the Viterbi algorithm is presented. Constant envelope digital modulation schemes with excellent spectral tail properties are given. The spectra have extremely low sidelobes. It is concluded that partial response CPM systems have spectrum compaction properties. Furthermore, at equal or even smaller bandwidth than minimum shift keying (MSK), a considerable gain in transmitter power can be obtained. This gain increases with M. Receiver and transmitter configurations are presented.**

I. INTRODUCTION

THIS paper presents constant envelope digital modulation systems having both good symbol error and spectral properties. The systems developed and studied are called partial response continuous phase modulation (CPM) systems. This is because the data symbols modulate the instantaneous phase of the transmitted signal and this phase is a continuous function of time. One single data symbol affects this phase over more than one symbol interval, an approach called *partial response signaling* [1], [3], [8]. The general class of signals is defined in Part I.

Previously, power spectra for systems of this type have been analyzed, for example, in [5], [9], and [14]. In this paper the analysis of the performance of the optimum detector for an additive white Gaussian channel is given. Some work on a suboptimum detector for a very special case of the CPM signaling scheme appears in [13].

As was treated in Part I of this paper, several attempts have been made to improve the asymptotic spectral properties for binary *full response* CPM systems with modulation index $h = 1/2$, compared to minimum shift keying (MSK). Considerable asymptotic improvement can be obtained by making the phase smoother at the bit transition instants, but even though the spectral properties with these schemes are asymptotically good, they are sometimes inferior to MSK for low and intermediate frequencies. But a result of Part I is that if full response CPM systems are to be used, a more attractive tradeoff between error probability performance and spectrum is achieved by using more levels than two and moderate smoothing of the phase at the symbol transition instants.

As will be shown in this paper, the use of partial response CPM systems yields a more attractive tradeoff between error probability and spectrum than does the full response systems. The spectral properties are improved at almost all frequencies and the first side-lobes are considerably lower. This spectral improvement takes place without increase of the probability of symbol error at practical signal to noise ratios. The improvement is obtained by introducing memory in the modulation process. The price for the improvements is system complexity, especially with respect to the optimum receiver. In practice, only rational values of the modulation index are useful, but it will be convenient here to imagine that h is real.

II. PROPERTIES OF THE MINIMUM EUCLIDEAN DISTANCE

In this section general properties of the minimum Euclidean distance as a function of the real valued modulation index h are given for partial response CPM systems. This distance is defined in Part I.

The Phase Tree and the Phase Difference Tree

An important tool for calculation of the minimum Euclidian distance is the so-called phase tree. This tree is formed by the ensemble of phase trajectories having a common start phase (root), say zero, at time $t = 0$. The data symbols for all the phase trajectories in the tree before this time are all equal. The value of these previous data symbols (the pre-history) can be chosen arbitrarily, but for unifying purposes they will be chosen to be $M - 1$; i.e., $\alpha_i = M - 1$; $i = -1, -2, \cdots$. An example of a phase tree for a binary partial response CPFSK system is shown in Fig. 1 and the frequency pulse $g(t)$ is

$$g(t) = \begin{cases} \dfrac{1}{6T}; & 0 < t < 3T \\ 0; & \text{otherwise.} \end{cases} \tag{1}$$

When a calculation of the minimum Euclidean distance is to be performed, the first pair of data symbols by definition must be different, and hence the phase trajectories are always different over this symbol interval. Going deeper into the tree however, it is always possible to find a pair of phase trajectories which coincide (modulo 2π) at a specific time, and do so ever after. This is called a merge. Denoting the time where the two phase trajectories merge by t_m, it can be seen that the calculation of the Euclidean distance only has to be performed over the interval $0 \leqslant t \leqslant t_m$; see (21), Part I.

Manuscript received March 19, 1980; revised September 19, 1980. This work was supported by the Swedish Board of Technical Development under Contract 79-3594.

T. Aulin and C.-E. W. Sundberg are with the Department of Telecommunication Theory, University of Lund, Fack, S-220 07, Lund, Sweden.

N. Rydbeck is with SRA Communications AB, S 163 00, Spånga, Sweden.

0090-6778/81/0300-0210$00.75

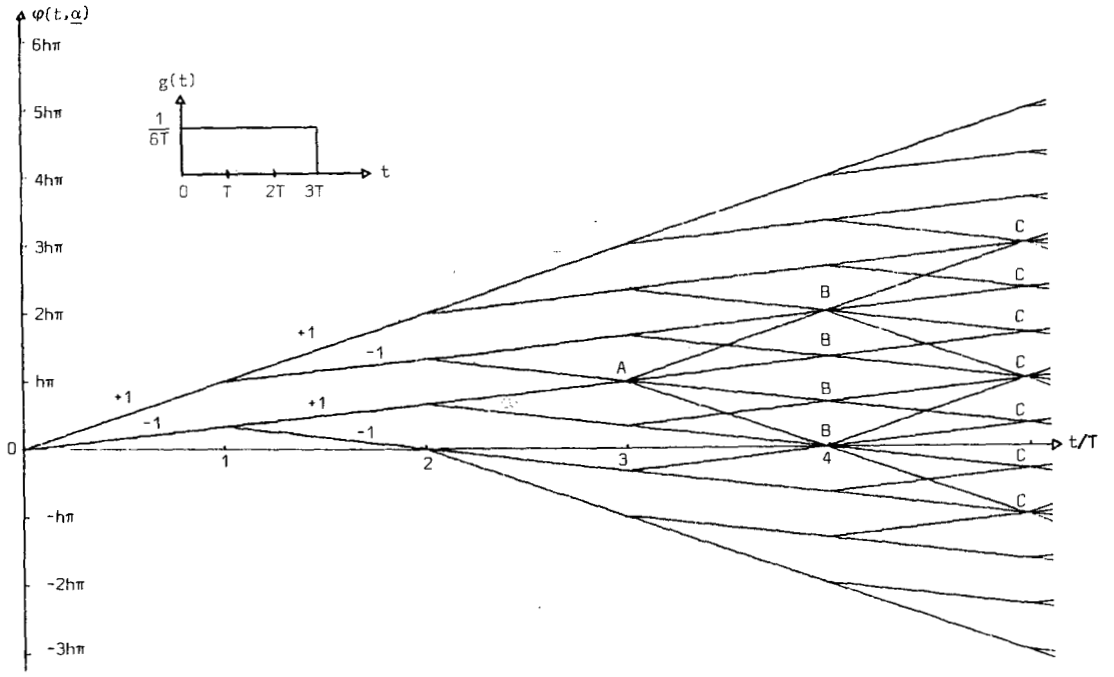

Fig. 1. Phase tree (ensemble of phase trajectories) when the frequency pulse $g(t)$ is constant and of length $L = 3$. It is assumed that all the binary ($M = 2$) data symbols prior to $t = 0$ are all +1. Note that A is a crossing and not a merge. B and C denotes first and second merges, respectively. Note: characters with underbars appear boldface in text.

The phase difference trajectories are defined by

$$\varphi(t, \underline{\gamma}) = 2\pi h \sum_{i=-\infty}^{\infty} \gamma_i q(t - iT);$$

$$\gamma_i = 0, \pm 2, \pm 4, \cdots, \pm 2(M-1). \tag{2}$$

The phase difference tree is now obtained from the ensemble of phase difference trajectories. Since the first pair of data symbols must be different in the phase tree, the first difference symbol γ_0 must not equal zero in the phase difference tree. In the phase tree the prehistory is the same for all phase trajectories, and thus the difference symbols forming the prehistory in the phase difference tree must all be zero. This means that the phase difference tree does not depend on the prehistory and hence, neither do the Euclidean distances (see (24), Part I).

Since there is a sign symmetry among the difference sequences and thus also among the phase difference trajectories, this can be removed for calculation of Euclidean distances. This is clear from I-(24) and the fact that cosine is an even function. For calculations of the minimum Euclidean distance, when the receiver observation interval equals N symbol intervals, it is sufficient to consider the phase difference tree, using the difference sequences $\underline{\gamma}_N$ defined by

$$\begin{cases} \gamma_i = 0 & i < 0 \\ \gamma_0 = 2, 4, 6, \cdots, 2(M-1) & \\ \gamma_i = 0, \pm 2, \pm 4, \cdots, \pm 2(M-1); & i = 1, 2, \cdots, N-1 \end{cases} \tag{3}$$

The merges are easily identified in the phase difference tree, since this corresponds to a phase difference trajectory which is identically equal to zero for all $t \geq t_m$.

In Fig. 2 the phase difference tree with sign symmetry removed is given for the frequency pulse defined by (1). Merges are also shown. Note that in Fig. 1 pairs of phase trajectories must be considered in calculating Euclidean distance, but in Fig. 2 only single phase difference trajectories need to be.

Weak Modulation Indices h_c

As was mentioned earlier, a phase difference trajectory identically equal to zero for all $t \geq t_m$ defines a merge. Since the phase difference tree always must be viewed modulo 2π in conjunction with distance calculations, a merge that depends upon the modulation index h is obtained if there exists a phase difference trajectory which equals a nonzero multiple of 2π for all $t \geq t_c$. The value of a phase difference trajectory depends on the modulation index h, and a situation like this occurs if

1) there exists a phase difference trajectory which is a constant not equal to zero for all $t \geq t_c$;

2) the modulation index h is chosen so that this constant is a multiple of 2π.

Since any phase difference trajectory is achieved by feeding the difference sequence into a filter having the impulse response $q(t)$ and multiplying the output of this filter by $2\pi h$, the first requirement is met for $t_c = LT$ by choosing

$$\gamma_i = \begin{cases} 0; & i < 0 \\ 2, 4, 6, \cdots, 2(M-1); & i = 0 \\ 0; & i > 0 \end{cases} \tag{4}$$

since for frequency pulses $g(t)$ of length L symbol intervals $q(t) = q(LT)$, $t \geq LT$. Sometimes this can occur also for $t_c =$

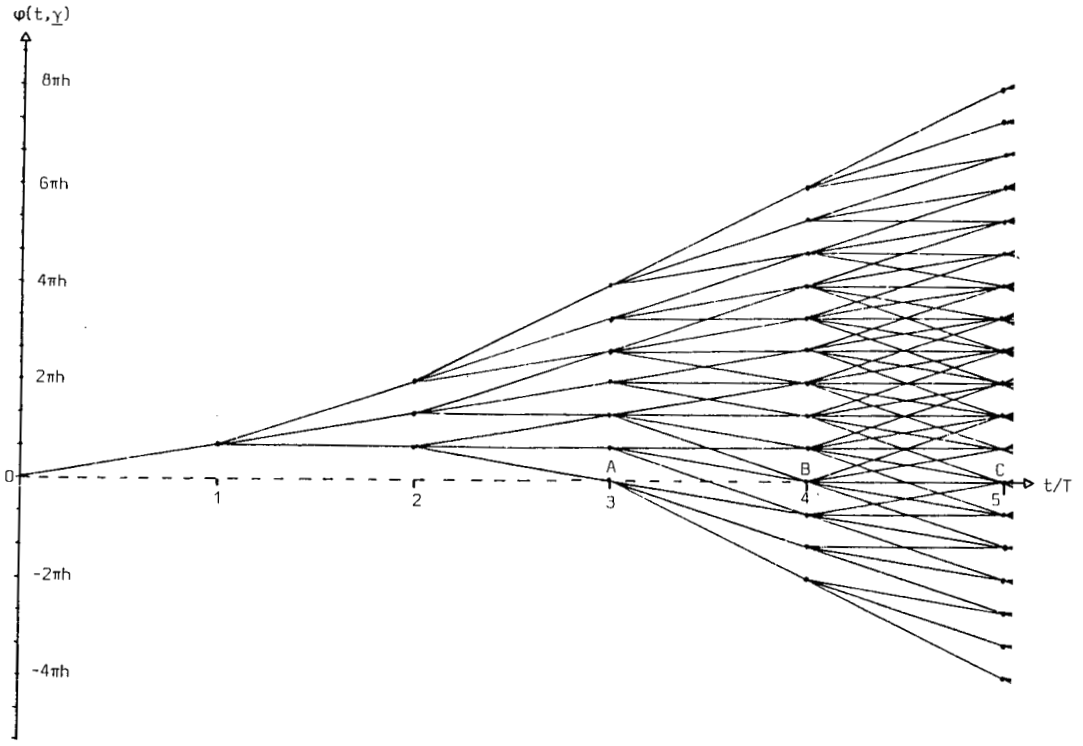

Fig. 2. Phase difference tree when the frequency pulse $g(t)$ is constant and of length $L = 3$ symbol intervals. Note that A is not a merge since the trajectory cannot be identically zero in the future. B and C denotes merges. Characters with underbars appear boldface in text.

$(L-1)T$, $(L-2)T$ and so on, but only for specific phase responses $q(t)$.

The second requirement above is satisfied if

$$2\pi h_c \gamma_0 q(LT) = k \cdot 2\pi; \quad k = 1, 2, \cdots \qquad \gamma_0 = 2, 4, 6, \cdots, 2(M-1) \tag{5}$$

where it is assumed that $q(LT) \neq 0$. Thus, for these modulation indices, in the sequel called *weak*, h_c satisfies

$$h_c = \frac{k}{\gamma_0 q(LT)}; \quad k = 1, 2, \cdots \qquad \gamma_0 = 2, 4, 6, \cdots, 2(M-1). \tag{6}$$

A merge, modulo 2π, occurs at $t = LT$.

In a similar way, the phase difference trajectory can be made constant for all $t \geq t_c = (L + \Delta L)T$ by choosing

$$\gamma_i = \begin{cases} 0; & i < 0 \\ 2, 4, 6, \cdots, 2(M-1); & i = 0 \\ 0, \pm 2, \pm 4, \cdots, \pm 2(M-1); & i = 1, 2, \cdots, \Delta L \\ 0; & i > \Delta L \end{cases} \tag{7}$$

and the weak modulation indices are

$$h_c = \frac{k}{q(LT) \sum_{i=0}^{\Delta L} \gamma_i}; \quad k = 1, 2, 3, \cdots \qquad q(LT) \neq 0 \qquad \sum_{i=0}^{\Delta L} \gamma_i \neq 0 \tag{8}$$

It can be noted that for a given finite interval of the modulation index, the number of weak modulation indices within this interval increases with M as in Part I.

In Fig. 3 the minimum normalized squared Euclidean distance is shown versus h when $N = 1, 2, \cdots, 10$ observed symbol intervals for the binary CPM system given by (1). It is seen that for most h the minimum Euclidean distance increases to an upper bound $d_B^2(h)$ with N, but not for the weak modulation indices

$$h_c = \tfrac{3}{4}, 1, \tfrac{9}{8}, \tfrac{6}{5}, \tfrac{9}{7}, \tfrac{3}{2}. \tag{9}$$

It can also be seen that some of the "weak" modulation indices, e.g., $h_c = 4/5$, $7/8$ do not affect the growth of the minimum Euclidean distance with N. This will be discussed in more detail later. However, indices such as $h_c = 3/2$ are catastrophic.

An Upper Bound on the Minimum Euclidean Distance

A phase difference trajectory identically equal to zero for all $t \geq t_m$ does not increase the Euclidean distance if the observation interval is made longer than $N = t_m/T$ symbol intervals. By choosing any fixed difference sequence so that a merge is obtained, a limited upper bound on the minimum Euclidean distance is obtained.

The first time instant for which any phase difference trajectory can be made identically zero ever after is in general $t = (L+1)T$, where L is the length of the causal frequency pulse $g(t)$. This is called the first merge, and the phase difference trajectories giving this merge are obtained by choosing the difference sequences

$$\gamma_i = \begin{cases} 0 & i < 0 \\ \gamma_0 = 2, 4, 6, \cdots, 2(M-1); & i = 0 \\ -\gamma_0 & i = 1 \\ 0 & i > 1 \end{cases} \tag{10}$$

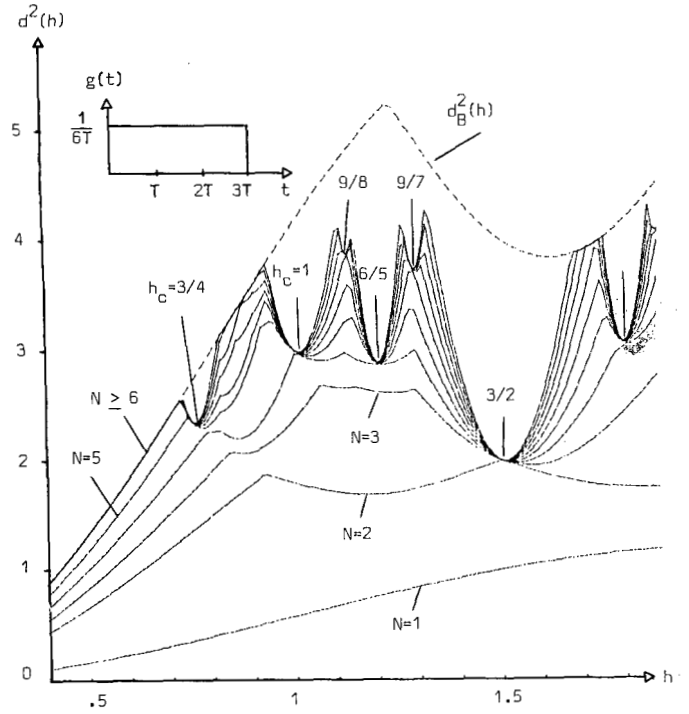

Fig. 3. The upper bound on the minimum Euclidean distance (dashed) and minimum distance curves (solid) for $1 \leqslant N \leqslant 10$ observed symbol intervals. The pulse $g(t)$ is constant and of duration $3T$ [equation (1)] and $M = 2$.

and thus the phase difference trajectories are

$$\varphi(t, \boldsymbol{\gamma}) = \begin{cases} 0; & t \leqslant 0 \\ \gamma_0 \cdot 2\pi h q(t); & 0 \leqslant t \leqslant T \\ \gamma_0 \cdot 2\pi h[q(t) - q(t-T)]; & T \leqslant t \leqslant (L+1)T \\ \gamma_0 \cdot 2\pi h[q((L+1)T) - q(LT)] = 0; & t \geqslant (L+1)T \end{cases} \tag{11}$$

By taking the minimum of the Euclidean distances between the signals having the phase difference trajectories above, an upper bound on the minimum Euclidean distance as a function of h, for fix M and $g(t)$, is achieved just as in Part I. The resulting bound is more complex, however.

One can also consider second merges, that is phase difference trajectories which merge at $t = (L + 2)T$. These phase difference trajectories are obtained from (2) by using

$$\gamma_i = \begin{cases} 0; & i < 0 \\ 2, 4, 6, \cdots, 2(M-1); & i = 0 \\ 0, \pm 2, \pm 4, \cdots, \pm 2(M-1); & i = 1, 2 \\ 0; & i > 2 \end{cases} \tag{12}$$

satisfying

$$\sum_{i=0}^{2} \gamma_i = 0. \tag{13}$$

It might happen that the Euclidean distance associated with these phase difference trajectories for a specific h is smaller than those giving the first merge. Hence, the former upper bound can be tightened by also taking the minimum of the Euclidean distances associated with the second merge. This new upper bound might also be further tightened by taking third merges into account, and so on.

The exact number of merges needed to give an upper bound on the minimum Euclidean distance which cannot be further tightened is not known in the general case, but in no case treated below were merges later than the Lth needed [16]-[18], [21]. For the full response case ($L = 1$) it was shown in Part I that first merges give the tight bound.

Fig. 3 shows the resulting upper bound dashed for the CPM scheme defined by (1) together with actual minimum normalized Euclidean distances when $N = 1, 2, \cdots, 10$ observed symbol intervals. The upper bound is the minimum of three functions corresponding to the first three merges [21].

As was mentioned earlier, not all weak modulation indices affect the minimum Euclidean distance. In this case the phase difference trajectories associated with (7) give larger Euclidean distances than the upper bound. Only those weak modulation indices which have phase difference trajectories having distance smaller than the upper bound affect the minimum Euclidean distance [21].

Weak Systems

In general, the first inevitable (independent of h) merge occurs at $t = (L + 1)T$. However, there are partial response CPM systems which have earlier merges, depending on the shape of the frequency pulse $g(t)$ and the number of levels M, but not the modulation index h. A partial response system is said to be *weak of order* L_c, if the first inevitable merge occurs at $t = (L + 1 - L_c)T$. L_c cannot be larger than L. A class of first-order weak systems are those where the frequency pulse $g(t)$ integrates to zero, i.e., $q(LT) = 0$. The sequence (10) of course still gives a merge, but not the earliest one. By choosing

$$\gamma_i = \begin{cases} 0; & i \neq 0 \\ \gamma_0 = 2, 4, 6, \cdots, 2(M-1); & i = 0 \end{cases} \tag{14}$$

the phase difference trajectory now equals zero for all $t \geqslant LT$; see (2). Examples of weak systems are given in [18] and [21]. The partial response CPFSK system having the frequency pulse

$$g(t) = \begin{cases} \dfrac{1}{4T}; & 0 < t < T \\ -\dfrac{1}{4T}; & T < t < 2T \\ 0; & \text{otherwise} \end{cases} \tag{15}$$

is a weak system of the first order [21].

The main conclusion concerning weak systems is that they should be avoided, since the potential maximum value of the minimum Euclidean distance, indicated by the upper bound $d_B^2(h)$, will never be reached due to the early merges. More results for weak systems can be found in [18]. We have found that there is little difficulty choosing pulses in such a way that the resulting schemes does not have the weak property considered above. This will be clearly illustrated in the following.

III. A SEQUENTIAL ALGORITHM FOR COMPUTATION OF THE MINIMUM EUCLIDEAN DISTANCE

A fast sequential algorithm for computation of the minimum Euclidean distance, for any real valued modulation index h and large numbers N of observed symbol intervals, has been developed. The algorithm is sequential in N and uses the basic properties of the minimum Euclidean distance, namely that it is upper bounded and is a nondecreasing function of N given $g(t)$, h, and M. The sequential property is obtained from the fact that squared Euclidean distances for coherent CPM systems are additive. This means that if the squared Euclidean distance has been calculated for N symbol intervals, the squared Euclidean distance for $N+1$ observed symbol intervals is obtained by just adding an increment to the previously calculated squared Euclidean distance. This holds for fixed difference sequences γ, and can be seen from the expression for the normalized squared Euclidean distance

$$d^2(\gamma_N, h) = N - \frac{1}{T}\sum_{i=0}^{N-1}\int_{iT}^{(i+1)T}\cos\left[2\pi h\left(\sum_{j=i-L+1}^{i}\gamma_j \cdot q(t-jT) + q(LT)\sum_{j=0}^{i-L}\gamma_j\right)\right]dt \tag{16}$$

Thus,

$$d^2(\gamma_{N+1}, h) = d^2(\gamma_N, h) + 1 - \frac{1}{T}\int_{NT}^{(N+1)T}\cos\left[2\pi h\left(\sum_{j=N-L+1}^{N}\gamma_j \cdot q(t-jT) + q(LT)\sum_{j=0}^{N-L}\gamma_j\right)\right]dt. \tag{17}$$

A brute force method for calculating the minimum Euclidean distance for a given N is to compute $d^2(\gamma_N, h)$ for all sequences γ_N defined by (3) and take the minimum of all the achieved quantities. The number of calculations required using this method grows exponentially with N since the number of difference sequences of length N is $(M-1)(2M-1)^{N-1}$ and even for $M=2$ it is unrealistic to calculate the minimum Euclidean distance for moderate N-values.

A flowchart for a more efficient algorithm can be seen in Fig. 4. It is assumed that the minimum Euclidean distance is to be calculated for a CPM system when the modulation index is $h = h_{\min}, h_{\min+\Delta h}, \cdots, h_{\max-\Delta h}, h_{\max}$ and for $1 \leqslant N \leqslant N_{\max}$ observed symbol intervals. The first step is to compute the upper bound $d_B{}^2(h)$ on the squared minimum Euclidean distance for the given h-values. Now all the Euclidean distances for $N=1$ observed symbol intervals are computed, i.e., the difference sequence if $\gamma_0 = 2, 4, \cdots, 2(M-1)$. If any of these distances is larger than the upper bound for that specific h-value, the entire subtree having the corresponding γ_0-value will never be used. This can be done since the Euclidean distance is a nondecreasing function of N for fixed h. The minimum of these Euclidean distances gives the minimum Euclidean distance over $N=1$ observed symbol intervals.

When the minimum Euclidean distance for $N=2$ observed symbol intervals is to be computed, only those γ_0-values whose corresponding distances when $N=1$ did not exceed the upper bound are used. The second component of the difference sequence is chosen to be $\gamma_1 = -2(M-1), -2(M-2), \cdots, 2(M-1)$, and the Euclidean distance is computed through (17). Again, only those sequences whose corresponding Euclidean distances are not above the upper bound will be stored as possible difference sequences for $N=3$. The algorithm continues like this up to the maximum N-value, $N_{\max}$. Through this procedure subtrees are continuously deleted.

It is clear that any finite upper bound on the minimum Euclidean distance can be used for cutting subtrees. If the upper bound is too loose, however, the number of possible difference sequences will grow. The algorithm will naturally be as fast as possible if the smallest possible upper bound is used.

This algorithm has empirically been found to increase only linearly in computational complexity with N, and not exponentially as the brute force method. Without this algorithm the results on the minimum Euclidean distances presented in the next chapter would be impossible to achieve. Using this algorithm allows observation intervals up to a couple of hundred symbol intervals, although $N \lesssim 100$ is usually sufficient.

IV. NUMERICAL RESULTS ON THE MINIMUM EUCLIDEAN DISTANCE

In the previous sections tools have been developed for evaluating the minimum Euclidean distance of any CPM system, and thus also the performance in terms of symbol error probability at large SNR. These tools will now be applied to selected classes of CPM systems. The chosen schemes are in no specific sense optimum. Systems are achieved, which are reasonably easy to describe and analyze and which have attractive properties.

The first class of partial response CPM systems analyzed in this chapter is defined by the frequency pulse

$$g(t) = \begin{cases} \dfrac{1}{2LT}\left(1-\cos\left[\dfrac{2\pi t}{LT}\right]\right); & 0 \leqslant t \leqslant LT \\ 0; & \text{otherwise,} \end{cases} \tag{18}$$

i.e., the frequency pulse $g(t)$ is a raised cosine over L symbol intervals. The class is obtained by varying M, L, and the modulation index h.

Another class of CPM systems which also will be considered are those having the Fourier transform of the frequency pulse $g(t)$

$$G(f) = F\{g(t)\} = \begin{cases} \dfrac{1}{4}\left(1+\cos\left[\dfrac{\pi f LT}{2}\right]\right); & |f| \leqslant \dfrac{2}{LT} \\ 0; & \text{otherwise,} \end{cases} \tag{19}$$

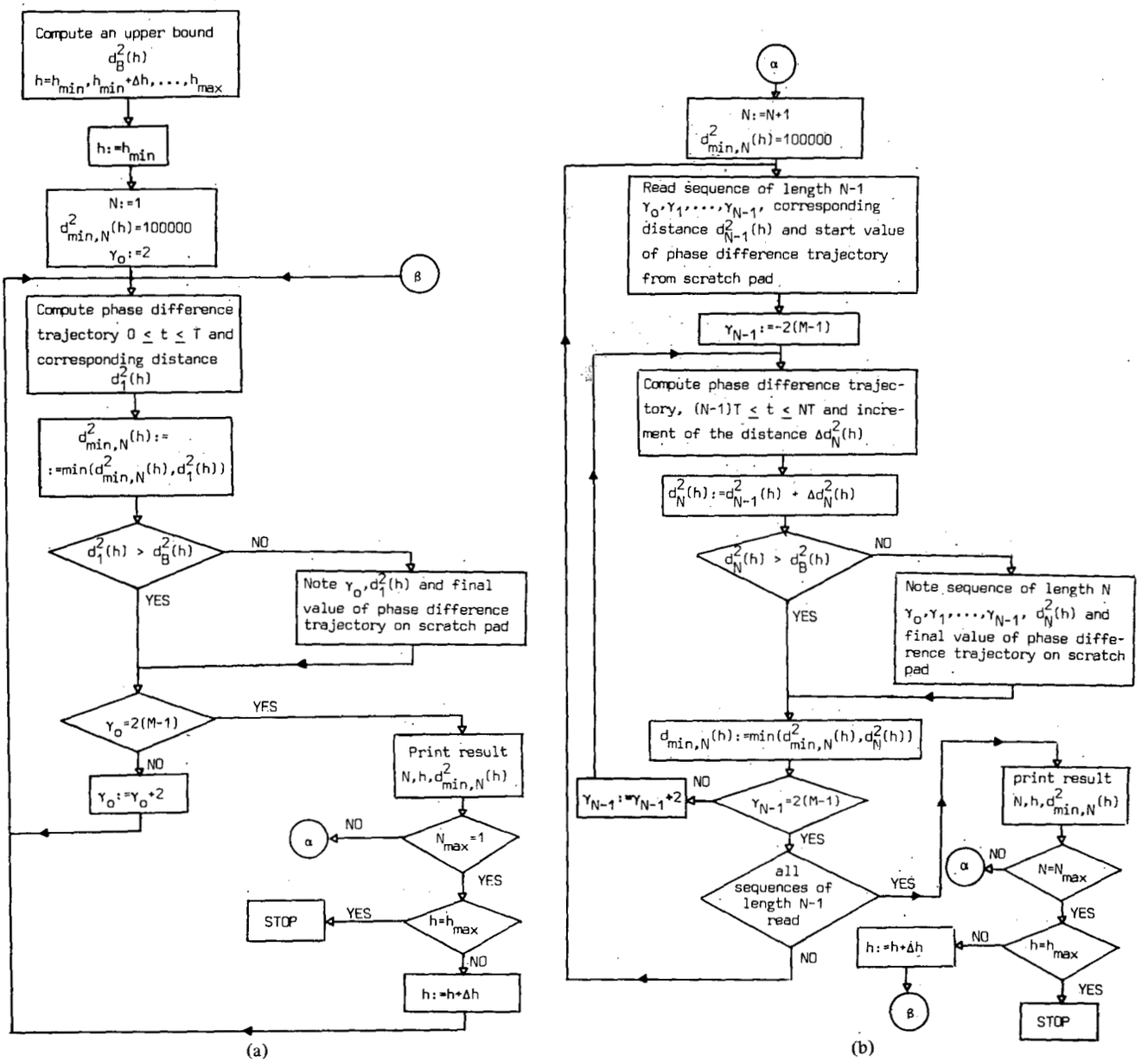

Fig. 4. (a) Flowchart for the sequential algorithm for computation of minimum distances $d^2_{\min,N}(h)$, $1 \leqslant N \leqslant N_{\max}$, $h_{\min} \leqslant h \leqslant h_{\max}$. (b) Continued.

i.e., the Fourier transform of the frequency pulse $g(t)$ is raised cosine shaped [4]. The frequency pulse is

$$g(t)=\frac{1}{LT}\,\frac{\sin\left[\dfrac{2\pi t}{LT}\right]}{\dfrac{2\pi t}{LT}}\cdot\frac{\cos\left[\dfrac{2\pi t}{LT}\right]}{1-4\left(\dfrac{2t}{LT}\right)^2} \tag{20}$$

which has an infinite duration. The third class of CPM systems has previously been considered [13] for the specific case $h = 1/2$, $M = 2$, and an approximation of the frequency pulse used is [17], [21]

$$g(t)=\tfrac{1}{8}\left[g_0(t-T)+2g_0(t)+g_0(t+T)\right] \tag{21}$$

where

$$g_0(t)\approx\frac{1}{T}\left[\frac{\sin(\pi t/T)}{\pi t/T}-\frac{\pi^2}{24}\cdot\frac{2\sin(\pi t/T)-(2\pi t/T)\cos(\pi t/T)-(\pi t/T)^2\sin(\pi t/T)}{(\pi t/T)^3}\right] \tag{22}$$

This scheme will be referred to as the TFM (tamed frequency modulation) system as in [13]. It will be analyzed only for the binary case, but the modulation index will not be constrained to 1/2 as in the approximate analysis presented in [13].

The schemes given by (18) will be denoted $1RC$ $(= RC)$,

$2RC$, $3RC$, etc. since the frequency pulse $g(t)$ is a raised cosine of length $L = 1, 2, 3$ etc. The schemes defined by (20) will be denoted $1SRC$, $2SRC$ etc. since the frequency pulse $g(t)$ has a Fourier transform which is raised cosine shaped (Spectral Raised Cosine) and the width of the main-lobe of this pulse is $L = 1, 2, 3$ etc.

Binary Systems

The RC class will now be analyzed by means of the minimum Euclidean distance. The simplest of these systems is naturally the $1RC$ scheme, which was considered in Part I. The minimum normalized squared Euclidean distance for the $2RC$ scheme is shown in Fig. 5 when the receiver observation interval is $N = 1, 2, 3, 4$, and 5 symbol intervals. The upper bound on the minimum Euclidean distance is shown dashed. For $h = 1/2$, all binary full response CPM systems including MSK have the minimum squared Euclidean distance 2 (see Part I). For this h-value the $2RC$ system yields almost the same distance when $N = 3$; the exact figure is 1.97. Hence, MSK and $2RC$ with $h = 1/2$ have almost the same performance in terms of symbol error probability for large SNR, but the optimum detector for the $2RC$ system must observe one symbol interval more than that for the MSK system. It can be expected, however, that the $2RC$, $h = 1/2$ system has a more compact spectrum due to its smooth phase tree, and this will be discussed in Section V.

For the binary full response CPFSK system, the maximum value of the minimum Euclidean distance is 2.43 when $h = 0.715$ and $N = 3$ [23]. Fig. 5 shows that larger values of the minimum Euclidean distance can be obtained for the $2RC$ system. When $h \approx 0.8$ the minimum Euclidean distance is 2.65 for $N = 4$. From a spectral point of view, however, low modulation indices should be used. It can be seen that in the region $0 < h \leqslant 1/2$, the upper bound is reached with $N = 3$ observed symbol intervals.

The phase tree for the binary $3RC$ system is shown in Fig. 6 and the specific shape of a phase depends upon the present and the two preceeding data symbols. This makes the phase tree yet smoother than for the $2RC$ case [20]. The first merge occurs at $t = 4T$. Note the straight lines in the phase tree. These occur for all RC-schemes and they can be used for synchronization [24], [28]. Note also that the slope in the phase tree is never larger than $h\pi/T$ (i.e., the slope of the full response CPFSK tree, Fig. 2 in Part I). This is true for all binary RC-schemes. The minimum normalized squared Euclidean distances for this scheme are shown in Fig. 7 when $N = 1, 2, \cdots, 6$ and $N = 15$ observed symbol intervals. The upper bound $d_B^2(h)$ has been calculated through the method described in Section III, using the first, second, and third merges.

For $N = 1$ observed symbol interval, the minimum Euclidean distance is very poor for almost every modulation index, but already with $N = 2$ it is increased significantly and when $N = 4$ the upper bound is reached in the region $0 < h \leq 1/2$. The upper bound in this region is lower than for the $2RC$ system, however. Outside this region larger minimum Euclidean distances can now be obtained, and for $h \approx 0.85$ the upper bound is reached with $N = 6$ observed symbol intervals and takes values around 3.35. The maximum value of the upper bound occurs for an h-value slightly smaller than $h = 1$.

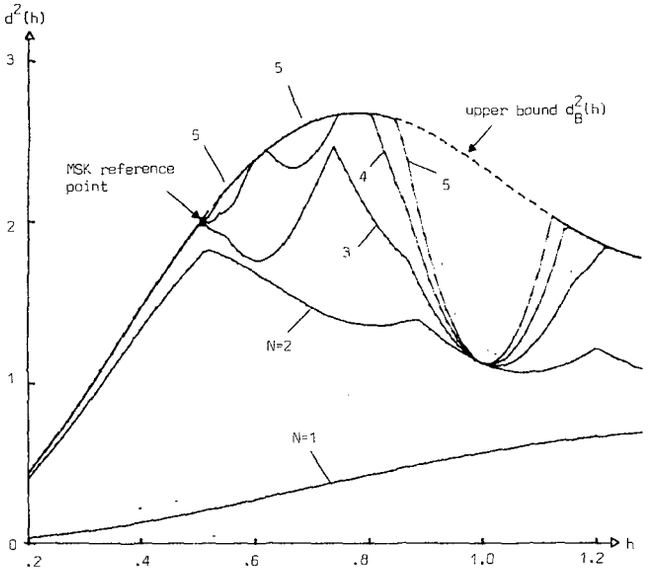

Fig. 5. Minimum squared Euclidean distance versus modulation index h for the binary $2RC$ scheme.

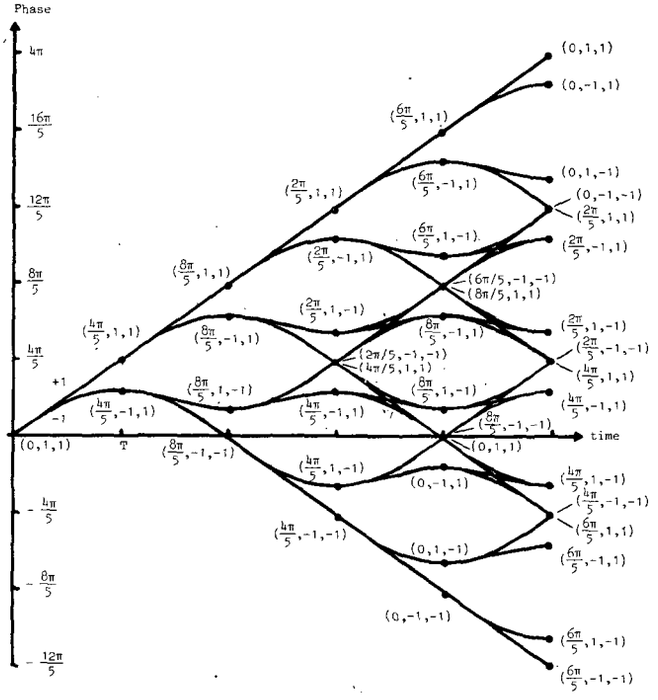

Fig. 6. Binary phase tree for $3RC$, $h = 4/5$. The assignment of states is used in Section VI.

There is an apparent weak modulation index when $h = 2/3$, but this is not a true weak modulation index since the minimun Euclidean distance in fact increases (by a small amount) when N is increased. This behavior is caused by a crossing and not a merge, and the phase trajectories are close after this crossing. The effect can be seen in the phase tree in Fig. 6, for this specific modulation index, if the phase is viewed modulo 2π.

Phase trees and minimum distance graphs for $4RC$, $5RC$ are found in [17], [20], and [21]. The distance/modulation index plot of the binary $6RC$ scheme is shown in Fig. 8. Note that the peak $d^2(h)$ value is larger than those for the shorter

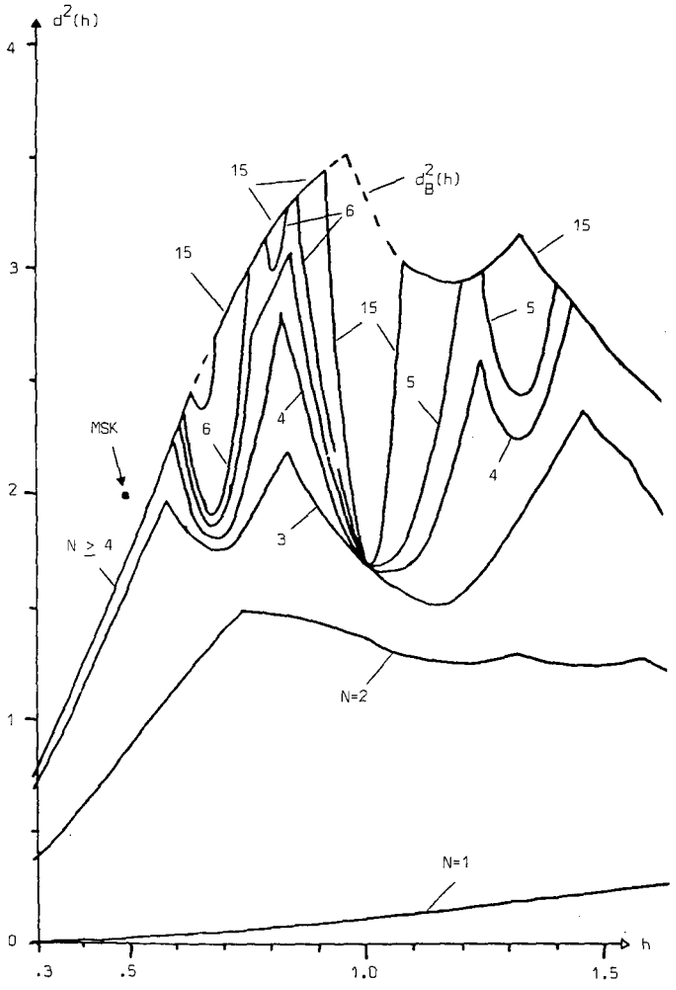

Fig. 7. Minimum squared Euclidean distance versus modulation index h for binary, $3RC$. N is the receiver observation interval. The upper bound is shown dashed.

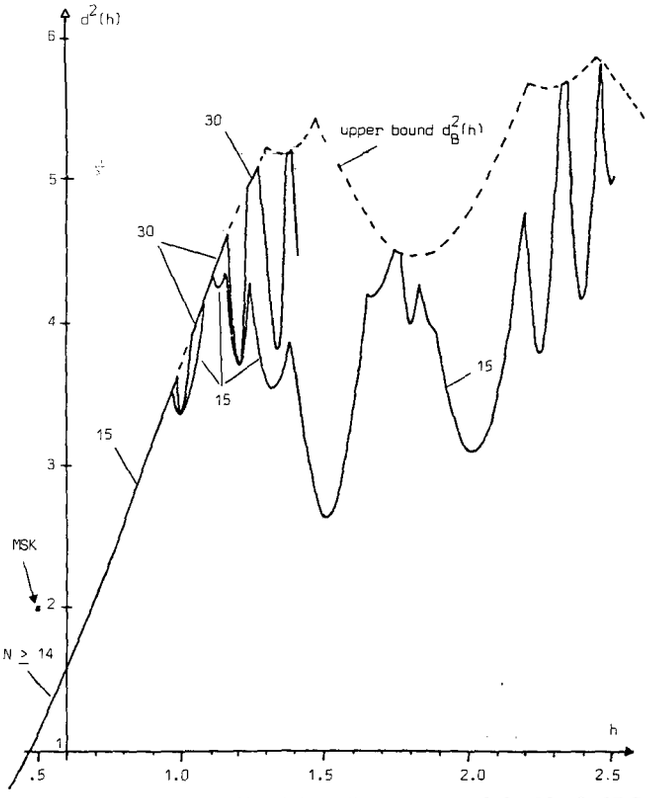

Fig. 8. Minimum squared Euclidean distance versus h for $M = 2$, $6RC$.

pulses and it occurs for a larger h-value. Also note that the distance value at h-values below 0.5 decreases with L. Fig. 8 also shows that longer pulses require longer observation intervals. For the binary $6RC$ system, minimum Euclidean distance values above 5 can be obtained when $h \approx 1.25$ and $N = 30$ observed symbol intervals. This corresponds to an asymptotic gain in SNR of at least 4 dB compared to MSK.

These trends are summarized in Fig. 9 using data in [17] and [21], where upper bounds for the RC family $3 \leqslant L \leqslant 6$ are shown. Except for a few weak h-values, the minimum distance equals $d_B{}^2(h)$ for sufficiently large N-values.

The binary system $8RC$ is second-order weak, i.e., the upper bound on the minimum Euclidean distance calculated by using the merge difference sequences can be further tightened by also taking into account the sequence giving the early merge at $t = 7T$. The two systems $7RC$ and $9RC$ are not weak according to the above definition, but since they are very close to the $8RC$ system they are "nearly weak." Thus, for $7RC$ and $9RC$ N must be chosen very large for all modulation indices to make the minimum Euclidean distance equal to the upper bound $d_B{}^2(h)$, even for very low h-values. For further details, see [17] and [21].

From a spectral point of view it is intuitively appealing to use strictly bandlimited frequency pulses $g(t)$. A frequently used pulse for digital AM-systems is the SRC pulse [4]. This pulse is of course of infinite duration.

The phase tree for the binary $3SRC$ system with the frequency pulse $g(t)$ given by (20) with $L = 3$ truncated symmetrically to a total length of 7 symbol intervals is very similar to the $3RC$ tree in Fig. 6. It is believed that an optimum detector for the $3RC$ system works well if the transmitted signal is $3SRC$, but the distortion in the $3SRC$ phase tree will appear as a slightly increased noise level. This assumption must of course be properly shown. Fig. 10 shows the minimum normalized squared Euclidean distances for the binary $3SRC$ scheme. The pulse $g(t)$ has been truncated to a total length of $7T$. By comparing these minimum Euclidean distances to those for the binary $3RC$ system (see Fig. 7), it is indeed seen that they are very similar. The number of observed symbol intervals required to reach the upper bound $d_B{}^2(h)$ must be increased for the $3SRC$ system, however. This is due to the tails of the $3SRC$ pulse.

A bandwidth efficient digital CPM system was recently developed and given the name tamed frequency modulation [13], or TFM. This binary system uses the bandlimited frequency pulse given by (21). This system has modulation index 1/2, and the detector is constructed with the assumption that the transmitted signal is linearly modulated, and is therefore suboptimum. The detector is simple, however, and simulations have indicated that the performance in terms of symbol error probability for a given SNR is very close to the optimum detector [13]. This system will now be analyzed by means of the minimum Euclidean distance; it has been generalized to include all real valued modulation indices. The result can be seen

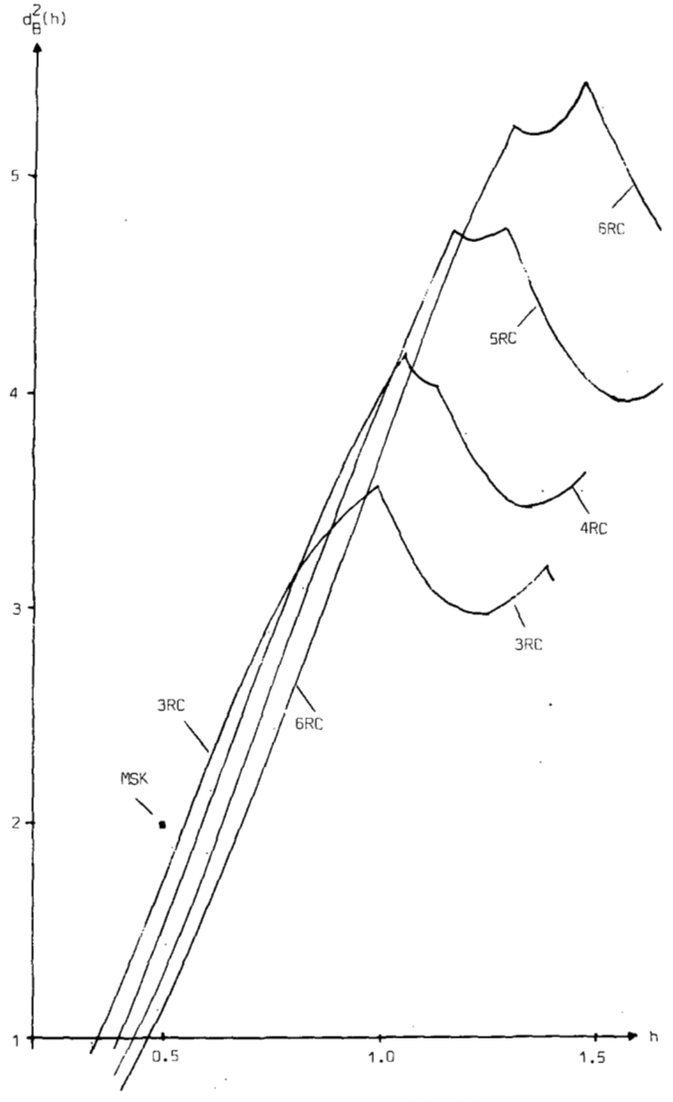

Fig. 9. Summary of upper bounds for 3*RC*-6*RC*. MSK is shown for comparison.

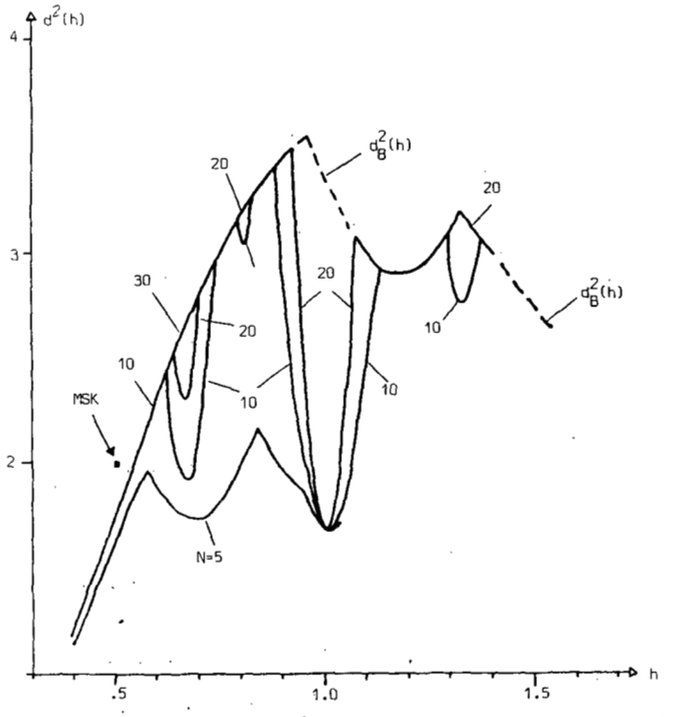

Fig. 10. Minimum squared Euclidean distances versus h for a binary modulation system with a spectral raised cosine pulse 3*SRC*, truncated to a total length of $7T$.

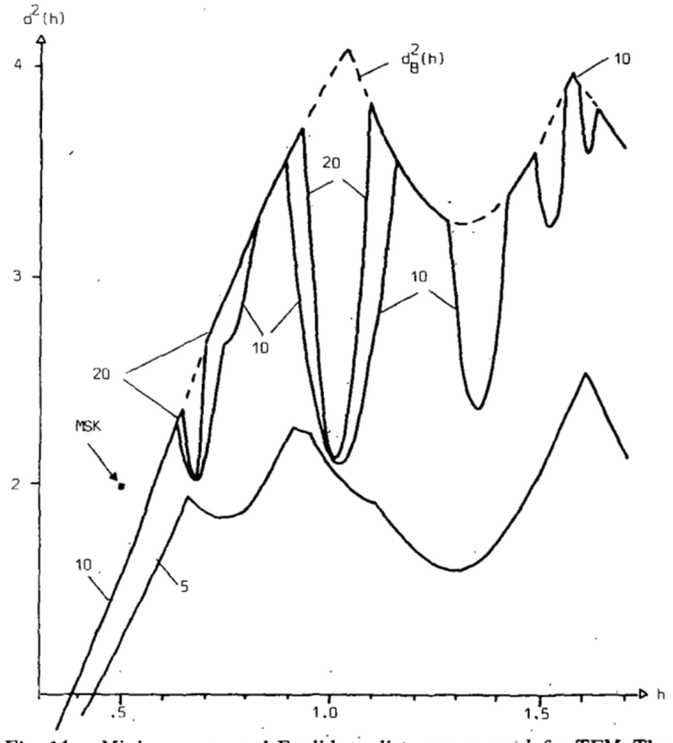

Fig. 11. Minimum squared Euclidean distances versus h for TFM. The subpulse $g_0(t)$ is truncated to a length of $5T$.

in Fig. 11. The subpulse $g_0(t)$ given by (22) has been truncated to a total length of five symbol intervals.

The main-lobe of the frequency pulse $g(t)$ used for the TFM system is approximatively $3.7T$. For $h = 1/2$ the upper bound on the minimum Euclidean distance is reached with $N = 10$ observed symbol intervals and equals 1.58. The value of the upper bound for 3*RC* and 4*RC* when $h = 1/2$ is 1.76 and 1.51, respectively.

Quaternary and Octal Systems

In Part I it was found that multilevel systems ($M = 4, 8, \cdots$) yield larger minimum Euclidean distances than binary systems. The first quaternary partial response CPM system within the *RC* class is 2*RC*. Now four phase branches leave every node in the phase tree, depending on the data symbols $\pm 1, \pm 3$. The phase tree for the binary 2*RC* system forms a subtree of the quaternary system. The first merges occur at $t = 3T$.

The result of the distance calculations, using the algorithm described in Section III, are shown in Fig. 12 for the $M = 4$, 3*RC* scheme. Distance calculations for various M-ary *RC* schemes are reported in [17] and [21]. The trends already observed for the binary system again appear as the length of the frequency pulse $g(t)$ is increased. The upper bound decreases for low modulation indices and increases for large modulation indices. Actually, very large values of the minimum

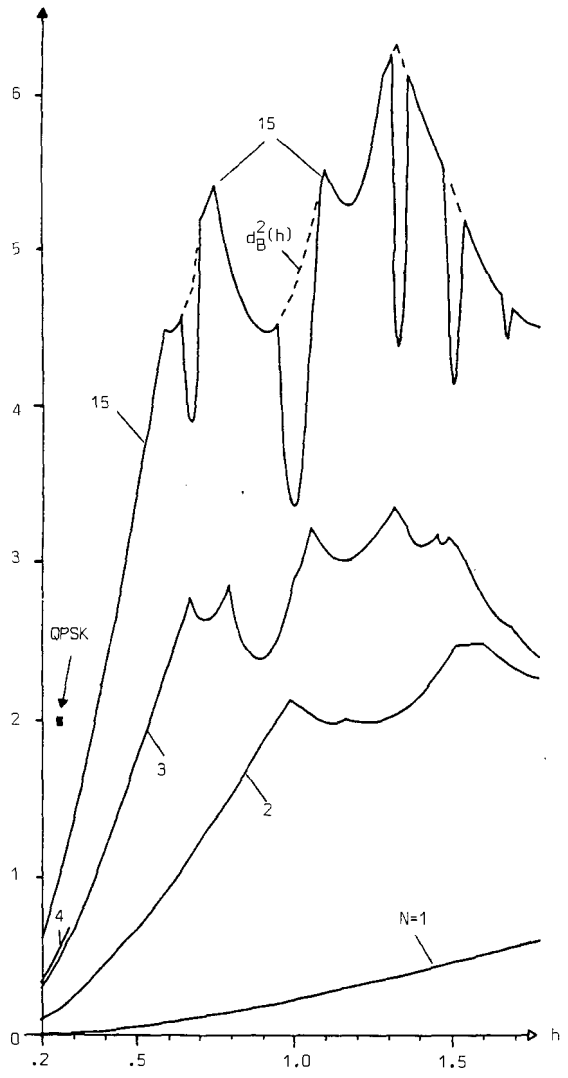

Fig. 12. Minimum squared normalized Euclidean distance versus h for $M = 4$, $3RC$. The upper bound is reached with $N = 12$ symbols in the interval $0.25 \leq h \leq 0.5$.

Euclidean distance are obtained in the region $h \approx 1.3$ and a receiver observation interval of $N = 15$ symbol intervals is enough to make the minimum Euclidean distance coincide with the upper bound. For these h-values the minimum Euclidean distance takes values around 6.28. This corresponds to an asymptotic gain of 5 dB compared to MSK or QPSK.

Minimum Euclidean distance calculations have also been performed for the octal ($M = 8$) and hexadecimal ($M = 16$) systems using the frequency pulses $2RC$ and $3RC$. The results can be found in [17] and [21]. The main conclusion concerning these results is that the trend for increasing L holds, i.e., lower values of $d_B^2(h)$ for low modulation indices, larger values of $d_B^2(h)$ for large modulation indices and an increased number of symbol intervals required in order to make the actual minimum Euclidean distance equal to the upper bound $d_B^2(h)$. The octal $3RC$ system yields a minimum Euclidean distance of 9.03 when $h = 1.38$ [21] with $N = 12$ symbol intervals required. The asymptotic gain in terms of E_b/N_0 compared to MSK or QPSK is 6.5 dB.

V. POWER SPECTRA

The power spectra (double-sided) can be obtained by numerical calculations, simulations in software, and hardware measurements. Numerical calculations have been carried out by using formulas in [25]. These computer calculations are very time consuming, especially for large M and L values and for large fT values. The bulk of the spectra in this paper have been obtained by means of simulations, a much faster method. For each pulse shape, M, h, and L value, the simulated spectra have been compared to numerically calculated spectra and a close fit was observed [26]. Comparisons have also been made to previously published numerically calculated spectra in [5], [9], and [14].

The simulated spectra have been calculated by the use of a well-tested simulation program [17]. In these simulations, which are made in discrete time, the complex envelope $e^{j\varphi(t,\alpha)}$ has been sampled four times per symbol interval. The data symbol sequence is a randomly generated 128 symbols long M-ary sequence, and the estimated power spectrum is the squared magnitude of the discrete Fourier transform (DFT) applied to the complex envelope $e^{j\varphi(t,\alpha)}$. These limitations introduce some distortion in the spectra and in some cases simulations have been performed using eight samples per symbol interval of the complex envelope. No significant change in the result has been observed.

The behavior of the power spectra for large frequencies is also of interest. It is not feasible to use the above-mentioned methods to obtain the spectral tail behavior due to numerical inaccuracy. In [5] the asymptotic behavior of partial response CPM systems is given. The number of continuous derivatives of $g(t)$ determines the fall-off rate for large frequencies [5], [26], as discussed below.

Fig. 13 shows the power spectra for the binary CPM systems $2RC$, $3RC$, and $4RC$ when $h = 1/2$. For comparison the spectrum for MSK is also shown. The frequency is normalized with the bit rate $1/T_b$, where $T = T_b \cdot \log_2 M$ and the spectra are shown in a logarithmic scale (dB). The spectrum for MSK falls off as $|f|^{-4}$ and for the RC-systems as $|f|^{-8}$ for large frequencies [5]. For full response CPM systems the improved fall-off rate has to be paid for by increased first side-lobes. It can be seen from Fig. 13, that by also increasing the length of the frequency pulse $g(t)$, the side-lobes can be made to decrease. The power spectra are thus compact and the first side-lobe very small with long pulses.

The effect of changing the modulation index h for the binary RC systems have been studied in detail in [17], [21], and [26]. The general trend is that the spectra become wider for increasing h-values, but normally maintain their smooth shape. As an example, see Fig. 14. For h-values equal to integer values, spectral lines occur [5], [25].

As can be expected, even more compact spectra can be obtained by using strictly bandlimited pulses $g(t)$ of the SRC-type. Fig. 15 shows the power spectra for the binary system $6SRC$, when the modulation index is $h = 0.4$, 0.5, 0.8, and 1.2. In this simulation the infinitely long frequency pulse given by (20) has not been significantly truncated [17]. It can be seen that these spectra are more compact than those for the

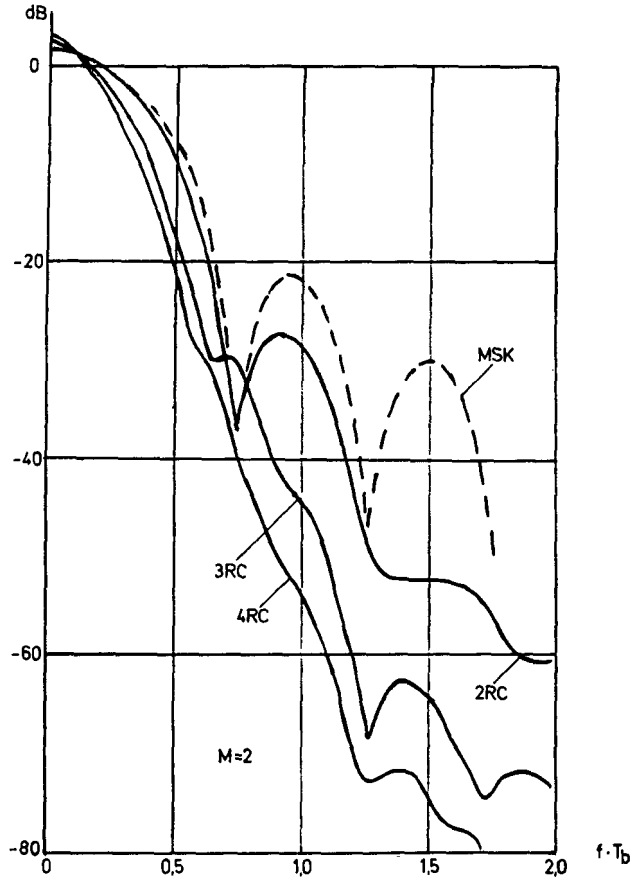

Fig. 13. Power spectra for binary CPM schemes with various baseband pulses. $h = 0.5$.

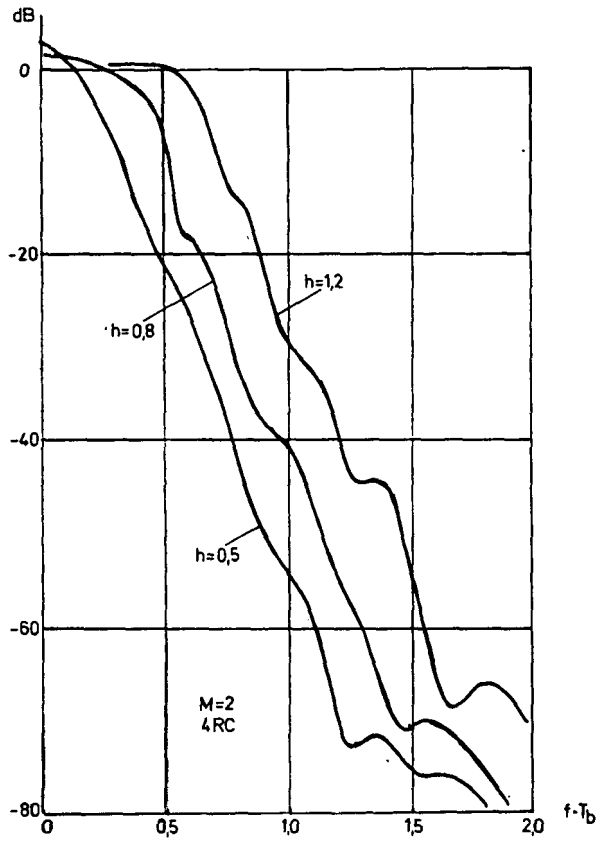

Fig. 14. Power spectra for $M = 2$, $4RC$. $h = 0.5$, 0.8, and 1.2.

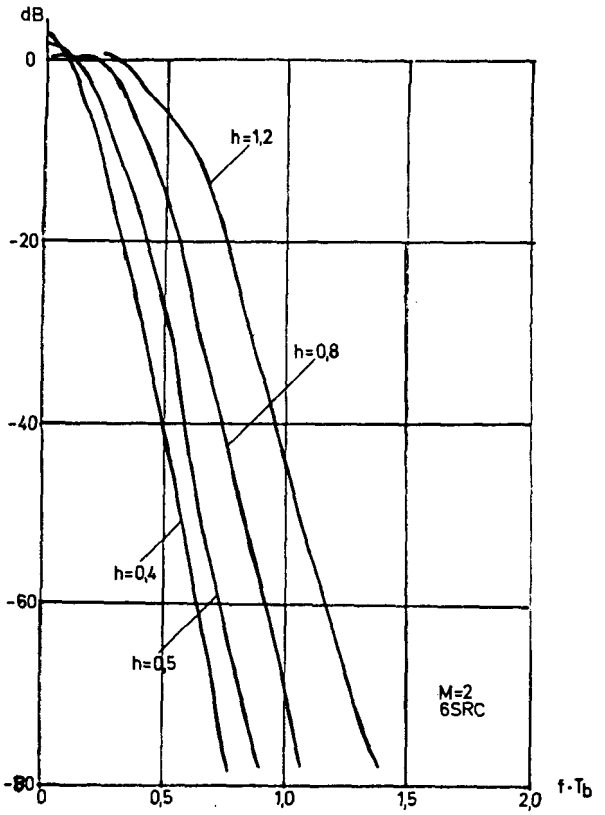

Fig. 15. Power spectra for $M = 2$, $6SRC$. No pulse truncation.

RC system for large frequencies. No side-lobes at all can be distinguished for the $6SRC$ spectra shown.

Bandwidth is not a quantity which is precisely defined for signals that are not strictly bandlimited. A common way of defining bandwidth for such signals is by means of the fractional out-of-band power (see Part I). Naturally, this definition of bandwidth can also be used for the CPM signals considered in this paper. However, since the power spectra are extremely compact and the out-of-band computation is not simple, bandwidth will instead be defined directly from the power spectra. Thus, the bandwidth $2BT_b$ is the bit rate normalized frequency for which the spectrum itself equals -60 dB when $f = B$. The level -60 dB has been chosen in order to illustrate constant envelope modulation schemes which have spectra sufficiently well-behaved to make bandlimiting radio-frequency filtering unnecessary.

Just like full response CPM systems multilevel partial response CPM systems yield more compact spectra than binary systems for fixed frequency pulse and distance. An example of this behavior is shown in Fig. 16, where the power spectra for the quaternary system ($M = 4$, $3RC$) is given for $h = 0.25, 0.4$, 0.5, and 0.6. By comparing to the corresponding binary systems, it can be seen that the spectra have been compressed by using four levels instead of two [17], [21]. Note that the frequency is normalized with the bit rate $1/T_b$ and not the symbol rate $1/T$.

Power spectra for multilevel systems having strictly bandlimited frequency pulses $g(t)$ are shown in [17] and [21]. The systems there are quaternary $3SRC$ and $4SRC$, and octal $3SRC$, respectively. For each of these systems spectra are shown for

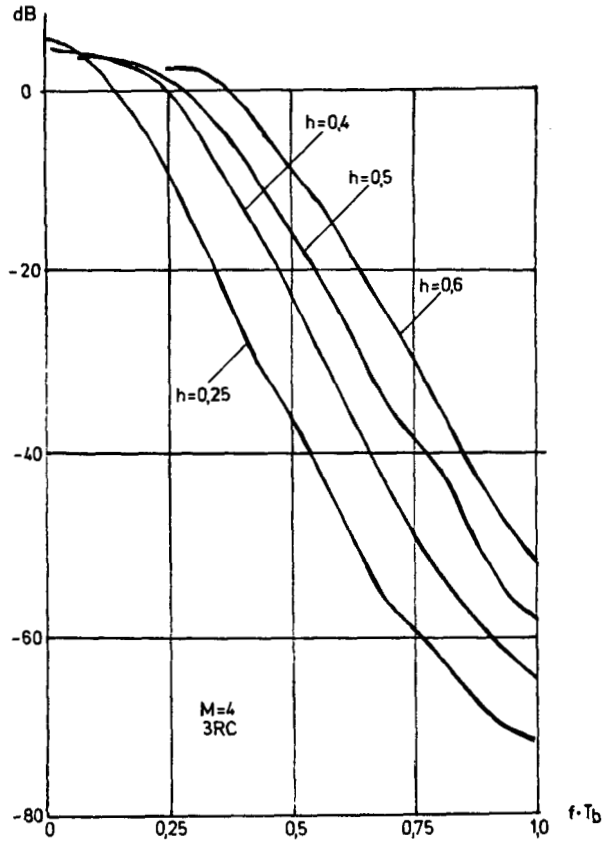

Fig. 16. Power spectra for $M = 4$, $3RC$. Note that the frequency is normalized with the bit rate $1/T_b$ in all spectrum figures.

various h-values. The same comparisons between the RC and the SRC schemes hold for the M-ary as for the binary case.

VI. TRANSMITTER AND RECEIVER STRUCTURES

It is assumed that the pulse $g(t)$ has finite length LT, i.e., $g(t) \equiv 0$ for $t < 0$ and $t > LT$. Since $g(t)$ is time limited, $q(t)$ is 0 for $t \leqslant 0$ and constant at $q(LT)$ for $t \geqslant LT$. For positive pulses $g(t)$, e.g., the raised cosine pulses (18), $q(LT) = 1/2$. Thus, the information carrying phase I-(5) can be written as

$$\varphi(t, \alpha) = 2\pi h \sum_{i=-\infty}^{n} \alpha_i q(t - iT)$$

$$= 2\pi h \sum_{i=n-L+1}^{n} \alpha_i q(t - iT) + h\pi \sum_{i=-\infty}^{n-L} \alpha_i,$$

$$nT \leqslant t \leqslant (n+1)T. \tag{23}$$

Hence, for given h and $g(t)$ and for any symbol interval n, the phase $\varphi(t, \alpha)$ is defined by α_n, the *correlative state vector* $(\alpha_{n-1}, \alpha_{n-2}, \cdots, \alpha_{n-L+1})$ and the *phase state* θ_n, where

$$\theta_n = h\pi \sum_{i=-\infty}^{n-L} \alpha_i \bmod 2\pi. \tag{24}$$

The number of correlative states is finite and equal to $M^{(L-1)}$. For rational modulation indices the phase tree is reduced to a phase trellis [10], [12], [22], [28]. For $h = 2k/p$ (k, p integers) there are p different phase states with values 0, $2\pi/p$, $2 \cdot 2\pi/p$, $\cdots$, $(p-1)2\pi/p$. The state is defined by the L-tuple $\sigma_n = (\theta_n, \alpha_{n-1}, \alpha_{n-2}, \cdots, \alpha_{n-L+1})$. The total number of states is $S = pM^{(L-1)}$. Transmitter and receiver structures utilizing these properties are described below.

Fig. 6 shows the phase tree for a binary system with a raised cosine pulse of length $L = 3$ ($3RC$) for $h = 4/5$. Phase states and correlative states are assigned to the nodes in the phase tree. The root node is arbitrarily given phase state 0. Each node in the tree is labeled with the state $(\theta_n, \alpha_{n-1}, \alpha_{n-2})$. The state trellis diagram can be derived from Fig. 6.

The transmitted signal can always be written

$$s(t, \alpha) = \sqrt{\frac{2E}{T}} [I(t) \cos(2\pi f_0 t) - Q(t) \sin(2\pi f_0 t)] \tag{25}$$

where

$$\begin{cases} I(t) = \cos[\varphi(t, \alpha)] \\ Q(t) = \sin[\varphi(t, \alpha)]. \end{cases} \tag{26}$$

From (23) we have

$$\varphi(t, \alpha) = \theta(t, \alpha) + \theta_n; \qquad nT \leqslant t \leqslant (n+1)T \tag{27}$$

where

$$\theta(t, \alpha) = 2\pi h \sum_{i=n-L+1}^{n} \alpha_i q(t - iT). \tag{28}$$

Hence, for $nT \leqslant t \leqslant (n+1)T$

$$\begin{cases} I(t) = \cos[\theta(t, \alpha)] \cos\theta_n - \sin[\theta(t, \alpha)] \sin\theta_n \\ Q(t) = \cos[\theta(t, \alpha)] \sin\theta_n + \sin[\theta(t, \alpha)] \cos\theta_n. \end{cases} \tag{29}$$

The basic transmitter structure is given by (25) and (26). The I- and Q-generators can be implemented in different ways. Fig. 17 shows an example based on (27) and (28). By also using (29), the ROM (read only memory) size can be reduced by a factor of p, but adders and multipliers must be used as in Fig. 18. Alternative structures are presented in [24]. These transmitters work for all rational h-values and time limited pulses $g(t)$. Only the ROM contents change. An exact rational relationship between h and $1/T$ is obtained. Both ROM's in Fig. 18 (phase branch ROM's) are of size $N_s \cdot N_q \cdot M^L$ bits, where N_s is the number of samples per symbol interval and N_q is the number of bits per sample. The size of the cos (θ_n) and sin (θ_n) ROM's is $p \cdot N_q$. The phase states are accessed sequentially [24].

From a spectral point of view it is desirable to use strictly bandlimited pulses $g(t)$, e.g., the SRC pulse given by (20). This pulse must be truncated to some length L_T, and hence the phase branch ROM's become a factor $M^{(L_T - L)}$ larger, compared to an RC pulse of length L.

Receiver Structures

The receiver observes the signal $r(t) = s(t, \alpha) + n(t)$, where the noise $n(t)$ is Gaussian and white (see Part I). The MLSE

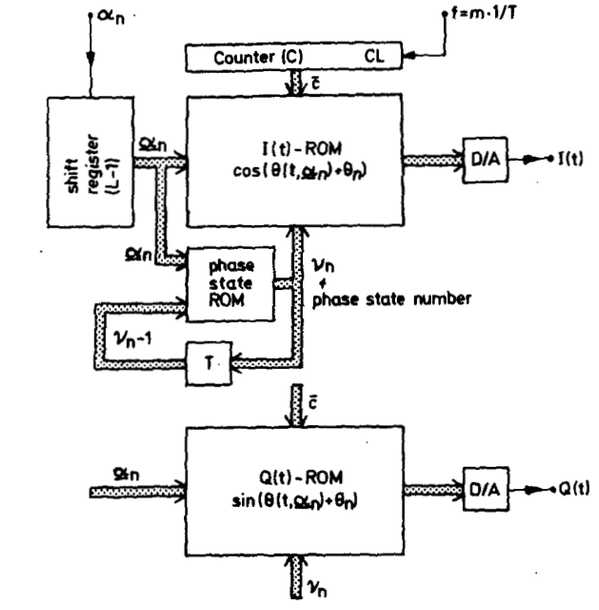

Fig. 17. I- and Q-generators. Characters with underbars appear boldface in text.

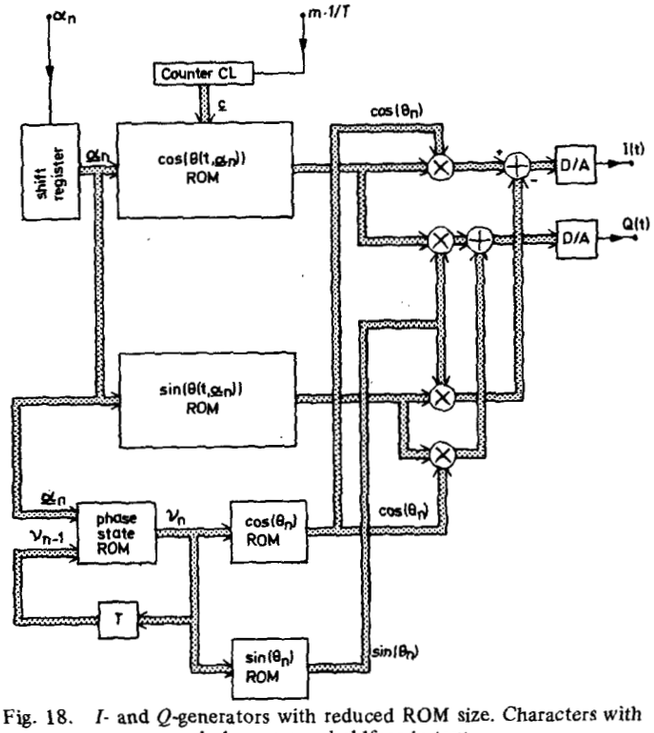

Fig. 18. I- and Q-generators with reduced ROM size. Characters with underbars appear boldface in text.

receiver maximizes the log likelihood function [2]

$$\log_e [p_{r(t)|\tilde{\alpha}}(r(t)|\tilde{\alpha})] \sim -\int_{-\infty}^{\infty} [r(t)-s(t,\tilde{\alpha})]^2\,dt \qquad (30)$$

with respect to the infinitely long estimated sequence $\tilde{\alpha}$. The maximizing sequence $\tilde{\alpha}$ is the maximum likelihood sequence estimate and $p_{r(t)|\tilde{\alpha}}$ is the probability density function for the observed signal $r(t)$ conditioned on the infinitely long sequence $\tilde{\alpha}$. It is equivalent to maximize the correlation

$$J(\tilde{\alpha}) = \int_{-\infty}^{\infty} r(t) \cdot s(t,\tilde{\alpha})\,dt. \qquad (31)$$

Now define

$$J_n(\tilde{\alpha}) = \int_{-\infty}^{(n+1)T} r(t) \cdot s(t,\tilde{\alpha})\,dt. \qquad (32)$$

Thus, it is possible to write

$$J_n(\tilde{\alpha}) = J_{n-1}(\tilde{\alpha}) + Z_n(\tilde{\alpha}) \qquad (33)$$

where

$$Z_n(\tilde{\alpha}) = \int_{nT}^{(n+1)T} r(t) \cdot \cos(\omega_0 t + \varphi(t,\tilde{\alpha}))\,dt. \qquad (34)$$

Using the above formulas it is possible to calculate the function $J(\tilde{\alpha})$ recursively through (33) and the metric $Z_n(\tilde{\alpha})$. This metric is recognized as a correlation between the received signal over the nth symbol interval and an estimated signal from the receiver.

The Viterbi algorithm [7] is a recursive procedure to choose those sequences that maximizes the log likelihood function up to the nth symbol interval. A trellis is used to choose among possible extensions of those sequences. The receiver computes $Z_n(\tilde{\alpha}_n, \tilde{\theta}_n)$ for all M^L possible sequences $\tilde{\alpha}_n = \{\tilde{\alpha}_n, \tilde{\alpha}_{n-1}, \cdots, \tilde{\alpha}_{n-L+1}\}$ and all p possible $\tilde{\theta}_n$. This makes $p \cdot M^L$ different Z_n values. Rewriting (34) using (27) yields

$$Z_n(\tilde{\alpha}_n, \tilde{\theta}_n) = \int_{nT}^{(n+1)T} r(t) \cdot \cos(\omega_0 t + \theta(t,\tilde{\alpha}_n) + \tilde{\theta}_n)\,dt. \qquad (35)$$

It is seen that $Z_n(\tilde{\alpha}_n, \tilde{\theta}_n)$ is obtained by feeding the signal $r(t)$ into a filter and sampling the output of the filter at $t = (n+1)T$. In this case a bank of bandpass filters must be used.

The noise $n(t)$ is written

$$n(t) = x(t) \cdot \cos\omega_0 t - y(t) \cdot \sin\omega_0 t. \qquad (36)$$

Using the basic quadrature receiver the received quadrature components are

$$\begin{cases} \hat{I}(t) = \dfrac{1}{2}\left[\sqrt{\dfrac{2E}{T}}\,I(t) + x(t)\right] \\ \hat{Q}(t) = \dfrac{1}{2}\left[\sqrt{\dfrac{2E}{T}}\,Q(t) + y(t)\right]. \end{cases} \qquad (37)$$

By inserting these components in (35) and omitting double

frequency terms, we have

$$
\begin{aligned}
&Z_n(\tilde{\alpha}_n, \tilde{\theta}_n) \\
&\quad = \cos(\tilde{\theta}_n) \int_{nT}^{(n+1)T} \hat{I}(t) \cdot \cos(\theta(t, \tilde{\alpha}_n))\, dt \\
&\qquad + \cos(\tilde{\theta}_n) \int_{nT}^{(n+1)T} \hat{Q}(t) \cdot \sin(\theta(t, \tilde{\alpha}_n))\, dt \\
&\qquad + \sin(\tilde{\theta}_n) \int_{nT}^{(n+1)T} \hat{Q}(t) \cdot \cos(\theta(t, \tilde{\alpha}_n))\, dt \\
&\qquad - \sin(\tilde{\theta}_n) \int_{nT}^{(n+1)T} \hat{I}(t) \cdot \sin(\theta(t, \tilde{\alpha}_n))\, dt. \qquad (38)
\end{aligned}
$$

This can be interpreted as $4M^L$ baseband filters with the impulse response

$$
h_c(t, \tilde{\alpha}_n) = \begin{cases} \cos\left[2\pi h \sum_{j=-L+1}^{0} \tilde{\alpha}_j q((1-j)T - t)\right] \\ 0 \quad \text{for } t \text{ outside } [0, T] \end{cases} \qquad (39)
$$

and

$$
h_s(t, \tilde{\alpha}_n) = \begin{cases} \sin\left[2\pi h \sum_{j=-L+1}^{0} \tilde{\alpha}_j q((1-j)T - t)\right] \\ 0 \quad \text{for } t \text{ outside } [0, T]. \end{cases} \qquad (40)
$$

The number of filters required can be reduced by a factor of two by observing that every $\tilde{\alpha}$-sequence has a corresponding sequence with reversed sign. Fig. 19 shows an optimum receiver with $F = 2M^L$ matched filters. The outputs of these filters are sampled once every symbol interval. The metrics $Z_n(\tilde{\alpha}_n, \tilde{\theta}_n)$ are obtained by the use of (38) and used by the Viterbi algorithm. A delay of N_T symbol intervals is introduced. Alternative receiver structures are given in [11], [12] and [24].

A method has been developed for calculation of upper bounds on the symbol error probability for a Viterbi detector having a path memory of length N_T symbol intervals [21], [27]. Fig. 20 shows the result of this calculation for the binary 3*RC* scheme with $h = 4/5$ when $N_T = 1, 2, \cdots, 20$ and $N_T = \infty$. A lower bound is also shown. As a reference the bit error probability for QPSK (BPSK) is shown dashed. The asymptotic behavior cannot be improved by making $N_T > N_B$ [27], where N_B is the value of N where $d^2_{\min} = {d_B}^2$. Compare the improvements of the upper bounds with N_T in Fig. 20 to the growth of $d^2_{\min}$ with N for $H = 4/5$ in Fig. 7.

The lower bound shown in Fig. 20 is based on the minimum Euclidean distance and it is seen that if $N_T \gtrsim N_B$, the upper and lower bounds are close even for fairly large error probabilities. By further increasing N_T, improvement is achieved for low SNR. For every low SNR the upper bounds are loose. From the calculation of $d^2_{\min}$ yielding the value 3.17 (see Fig. 7), the asymptotic gain in E_b/N_0 is 2.00 dB compared to QPSK(MSK). From Fig. 20, it is seen that this gain is achieved even at fairly low SNR. This conclusion holds for a large variety of schemes and it can thus be concluded that the minimum Euclidean distance is sufficient for the characterization of performance in terms of symbol error probability [21], [27]. Even where the upper bound is loose the minimum distance appears to be accurate. For the scheme considered in Fig. 20 some simulation results are shown. In this simulation a coherent Viterbi detector with $N_T = 11$ was used. We have obtained results similar in appearance for a wide variety of modulation systems [21].

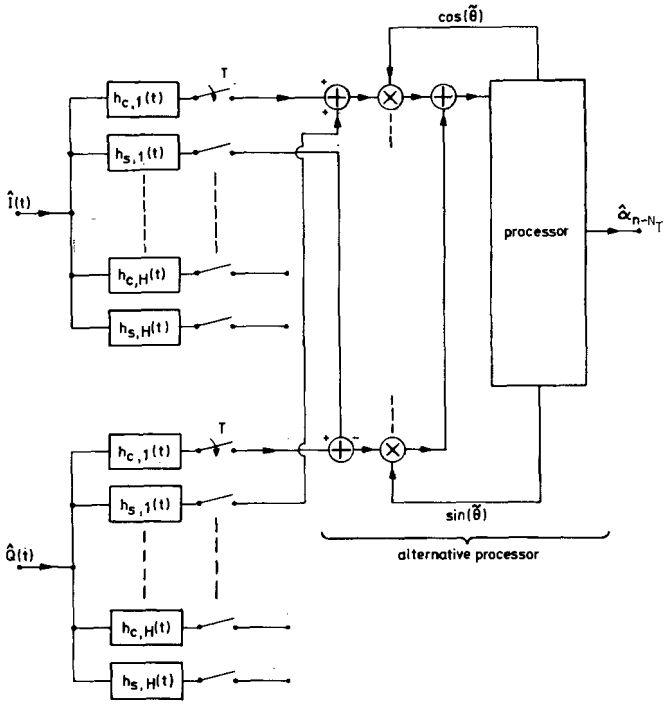

Fig. 19. Matched filter receiver. $H = F/4$.

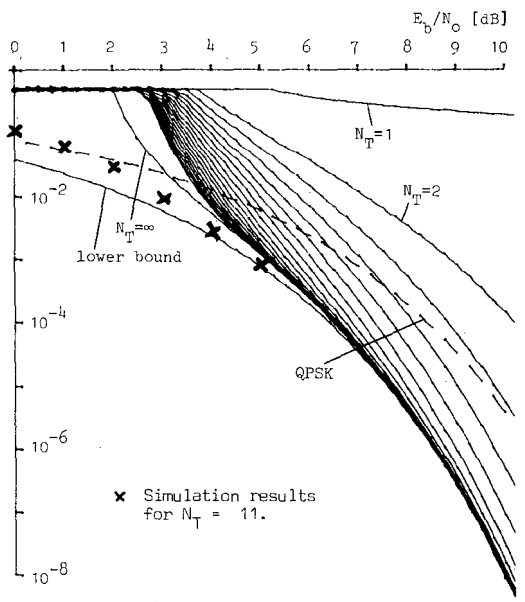

Fig. 20. Upper bounds on the bit error probability for 3*RC*, $M = 2$, $h = 4/5$. A lower bound is also shown. Compare QPSK (dashed).

VII. DISCUSSION AND CONCLUSIONS

In this paper classes of M-ary partial response CPM systems have been analyzed, with respect to their minimum Euclidean distance, error probability, and spectral properties. Naturally it is desirable to have a system which yields both large values of the minimum Euclidean distance (small error probability) and a compact spectrum. To start with binary systems, the RC schemes give lower values of the upper bound on the minimum Euclidean distance for low h-values and larger for large h-values. To have an RC system with main-lobe width L bit intervals with the same performance as MSK for large SNR, the modulation index must be chosen larger and larger as L is increased. For the $3RC$ system h must be 0.56 roughly, and for the $4RC$ system, about .60. Although the modulation index is slightly increased, the spectra for the two partial response systems are far more attractive than that for MSK. This is true also for the asymptotic spectral behavior. At $f \cdot T_b = 1$ the spectrum for $3RC$ with $h = 0.56$ is 23 dB lower than the MSK spectrum and the corresponding figure for $4RC$ with $h = 0.6$ is 33 dB. For the $5RC$ system, the modulation index must be $h \approx .63$ to have the minimum Euclidean distance 2, i.e., the same as MSK. The spectral behavior of the system $5RC$ with $h \approx 0.63$ is far more compact than for the MSK system and at $f \cdot T_b = 1$ there is a 40 dB difference in favor for the RC system. This is a clear trend: Using RC systems with longer frequency pulses and with the modulation index chosen to yield the same performance in terms of error probability for large SNR as MSK, spectrally more efficient systems are obtained. The number of observed symbol intervals must grow however.

Binary RC systems can also be chosen which yield large gains in E_b/N_0. Take the $6RC$ with $h = 1.28$. When $N = 30$ observed bit intervals a gain of 4 dB in E_b/N_0 is obtained compared to MSK. When $|f \cdot T_b| \gtrsim 0.8$ the spectrum for $6RC$ with $h = 1.28$ is below the MSK spectrum, and the asymptotic properties of the $6RC$ spectrum are of course more attractive.

If a smaller minimum Euclidean distance than two can be accepted, which is sometimes the case, still narrower band binary RC schemes can be considered. For example, the binary RC systems with minimum Euclidean distance 1/2 have a loss of 6 dB in E_b/N_0. Systems having this performance are $2RC$, $h \approx 0.21$; $3RC$, $h \approx 0.25$; $6RC$, $h \approx 0.34$. These systems are very narrow band.

The favorable minimum Euclidean distance versus bandwidth tradeoff pointed out for a few cases of binary partial response CPM is even more pronounced for systems using more levels than two. Quaternary RC systems having the same minimum Euclidean distance as MSK are $2RC$, $h \approx 0.32$, and $3RC$, $h \approx 0.37$. From [21], the quaternary systems give more compact spectra for the same distance. The octal system $2RC$, $h \approx 0.25$ and the hexadecimal system $2RC$, $h \approx 0.21$ yield the same minimum Euclidean distance as MSK. The modulation indices are very low and thus good spectral properties can be expected.

Large gains in terms of E_b/N_0 can be achieved especially for multilevel systems, and as an example the system $M = 8$, $3RC$, $h \approx 1.38$ is chosen. With $N = 12$ observed symbol intervals the minimum normalized square Euclidean distance equals 9.03, and thus the gain in E_b/N_0 for large SNR is 6.5 dB.

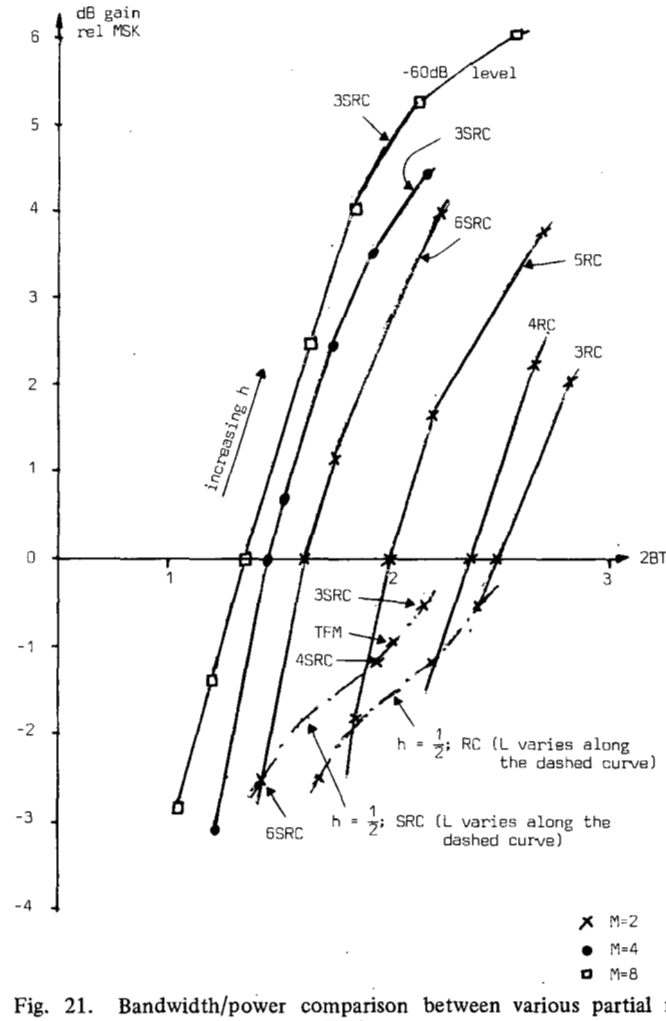

Fig. 21. Bandwidth/power comparison between various partial response CPM systems.

A summary of results concerning the bandwidth–minimum Euclidean distance tradeoff is given in Fig. 21. The bandwidth has been calculated using the definition in Section V, i.e., the double-sided bit rate normalized frequency where the double-sided power spectrum takes the value –60 dB. This figure shows the asymptotic gain in E_b/N_0 compared to MSK (and QPSK) versus the corresponding bandwidth for a number of M-ary partial response CPM schemes. For example, for the scheme $M = 8$, $3SRC$ a number of bandwidth and distance values are shown as □ in the figure. To underline the fact that only h varies, but that the pulse shape and the number of levels are the same, these points are connected. The interaction between distance and bandwidth for a fixed scheme when h varies is clearly demonstrated. The figure also shows the clear improvement which is obtained by increasing L and/or M. Another trend shown in Fig. 21 is the connection between binary RC and SRC schemes for $h = 1/2$ and increasing L. Both bandwidth and distance change with L for fixed h. Plots like figure 21 can be drawn for alternative definitions of bandwidth, depending on the application. The plots will be different, but the relative positions of the different schemes will remain unchanged.

The main conclusion concerning the systems considered in this paper is that digital constant envelope modulation systems can be found which are both power and bandwidth efficient. Nonbinary (e.g., $M = 4$) systems are especially attractive. A specific system is achieved by specifying the number of levels M, the modulation index h, and the frequency pulse $g(t)$. The modulation index should be rational for implementation reasons. The price that has to be paid for systems with optimum receivers is complexity.

REFERENCES

[1] A. Lender, "The duobinary technique for high speed data transmission," *IEEE Trans. Commun. Electron.*, vol. COM-11, pp. 214–218, May 1963.

[2] J. M. Wozencraft and I. M. Jacobs, *Principles of Communication Engineering*. New York: Wiley, 1965.

[3] A. Lender, "Correlative level coding for binary data transmission," *IEEE Spectrum*, vol. 3, pp. 104–115, Feb. 1966.

[4] R. W. Lucky, J. Salz, and E. J. Weldon, *Principles of Data Communication*. New York: McGraw-Hill, 1968.

[5] T. J. Baker, "Asymptotic behavior of digital FM spectra," *IEEE Trans. Commun.*, vol. COM-22, pp. 1585–1594, Oct. 1974.

[6] W. C. Lindsey and M. K. Simon, *Telecommunication Systems Engineering*. Englewood Cliffs, NJ: Prentice-Hall, 1974.

[7] G. D. Forney, "The Viterbi algorithm," *Proc. IEEE*, vol. 61, pp. 268–278, Mar. 1973.

[8] P. Kabal and S. Pasupathy, "Partial response signaling," *IEEE Trans. Commun.*, vol. COM-23, pp. 921–934, Sept. 1975.

[9] G. J. Garrison, "A power spectral density analysis for digital FM," *IEEE Trans. Commun.*, vol. COM-23, pp. 1228–1243, Nov. 1975.

[10] J. B. Anderson and R. de Buda, "Better phase-modulation error performance using trellis phase codes," *Electron. Lett.*, vol. 12, pp. 587–588, Oct. 1976.

[11] R. C. Davis, "An experimental 4-ary CPFSK modem for line-of-sight microwave digital data transmission," in *EASCON Conf. Rec.*, Washington, DC, 1978, pp. 674–682.

[12] T. A. Schonhoff, H. E. Nichols, and H. M. Gibbons, "Use of the MLSE algorithm to demodulate CPFSK," in *Proc. Int. Conf. Commun.*, Toronto, Canada, 1978, pp. 25.4.1–25.4.5.

[13] F. deJager and C. B. Dekker, "Tamed frequency modulation, a novel method to achieve spectrum economy in digital transmission," *IEEE Trans. Commun.*, vol. COM-26, pp. 534–542, May 1978.

[14] G. S. Deshpande and P. H. Wittke, "The spectrum of correlative encoded FSK," in *Proc. Int. Conf. Commun.*, Toronto, Canada 1978, pp. 25.3.1–25.3.5.

[15] T. Aulin, N. Rydbeck, and C-E. Sundberg, "Bandwidth efficient digital FM with coherent phase tree demodulation," Telecommun. Theory, Univ. of Lund, Lund, Sweden, Tech. Rep. TR-102, May 1978.

[16] ——, "Bandwidth efficient constant-envelope digital signalling with phase-tree demodulation," *Electron. Lett.*, vol. 14, pp. 487–489, July 1978.

[17] ——, "Further results on digital FM with coherent phase tree demodulation–minimum distance and spectrum," Telecommun. Theory, Univ. of Lund, Lund, Sweden, Tech. Rep. TR-119, Nov. 1978.

[18] T. Aulin and C-E. Sundberg, "Minimum distance properties of M-ary correlative encoded CPFSK," Telecommun. Theory, Univ. of Lund, Lund, Sweden, Tech. Rep. TR-120, Nov. 1978.

[19] N. Rydbeck and C-E. Sundberg, "Recent results on spectrally efficient constant envelope digital modulation methods," in *Proc. IEEE Int. Conf. Commun.*, Boston, MA, 1979, pp. 42.1.1–42.1.6.

[20] T. Aulin, N. Rydbeck, and C-E. Sundberg, "Bandwidth efficient digital FM with coherent phase tree demodulation," in *Proc. IEEE Int. Conf. Commun.*, Boston, MA, 1979, pp. 42.4.1–42.4.6.

[21] T. Aulin, "CPM—A power and bandwidth efficient digital constant envelope modulation scheme," Ph.D. dissertation, Telecommun. Theory, Univ. of Lund, Lund, Sweden, Nov. 1979.

[22] T. Aulin, N. Rydbeck, and C-E. Sundberg, "Performance of constant envelope M-ary digital FM-systems and their implementation," in *Proc. Nat. Telecommun. Conf.*, Washington, DC, 1979, pp. 55.1.1–55.1.6.

[23] T. Aulin and C-E. Sundberg, "Continuous phase modulation—Part I: Full response signaling," this issue, pp. 196–209.

[24] T. Aulin, N. Rydbeck, and C-E. Sundberg, "Transmitter and receiver structures for M-ary partial response FM. Synchronization considerations," Telecommun. Theory, Univ. of Lund, Lund, Sweden, Tech. Rep. TR-121, June 1979.

[25] R. R. Anderson and J. Salz, "Spectra of digital FM," *Bell Syst. Tech. J.*, vol. 44, pp. 1165–1189, July–Aug. 1965.

[26] T. Aulin and C-E. Sundberg, "Digital FM spectra–Numerical calculations and asymptotic behaviour," Telecommun. Theory, Univ. of Lund, Lund, Sweden, Tech. Rep. TR-141, May 1980.

[27] T. Aulin, "Symbol error probability bounds for coherently Viterbi detected digital FM," Telecommun. Theory, Univ. of Lund, Lund, Sweden, Tech. Rep. TR-131, Oct. 1979.

[28] T. Aulin, N. Rydbeck, and C-E. Sundberg, "Transmitter and receiver structures for M-ary partial response FM," in *Proc. 1980 Int. Zürich Seminar on Digital Commun.*, Mar. 4–6, 1980, pp. A2.1–A2.6.

★

Tor Aulin (S'77–M'80), for a photograph and biography, see this issue, p. 195.

★

Nils Rydbeck, for a photograph and biography, see this issue, p. 195.

★

Carl-Erik W. Sundberg (S'69–M'75), for a photograph and biography, see this issue, p. 195.